Reconstructing entanglement Hamiltonian via entanglement eigenstates

W. Zhu, Zhoushen Huang, and Yin-Chen He

Phys. Rev. B **99**, 235109 — Published 4 June 2019

DOI: 10.1103/PhysRevB.99.235109

Reconstructing Entanglement Hamiltonian via Entanglement Eigenstates

W. Zhu[1,2], Zhoushen Huang[1], Yin-Chen He[3,4]
[1] *Westlake Institute of Advanced Study, Hangzhou, 310024, P. R. China*
[2] *Theoretical Division, Los Alamos National Laboratory, Los Alamos, NM 87545, USA*
[3] *Department of Physics, Harvard University, Cambridge MA 02138 and*
[4] *Perimeter Institute for Theoretical Physics, Waterloo, Ontario N2L 2Y5, Canada*

Entanglement Hamiltonian holds crucial clues in understanding quantum entanglement and its underlying phenomenon in strongly-correlated systems. To date, however, a generic recipe to map out the operator form of entanglement Hamiltonian remains outstanding. Here, we present a systematic framework which explicitly reconstructs entanglement Hamiltonian based on the information of one entangled mode of the reduced density matrix. We demonstrate its successful application to quantum spin lattice models. The obtained entanglement Hamiltonians accurately recover the expectations from analytical theories and faithfully capture all features of the reduced density matrices, which are evidenced by the agreement between the original and reconstructed full entanglement spectra and the high density matrix fidelity.

Introduction.— Entanglement-based analysis continually brings inspirational insights into the study of condensed matter systems, particularly those with strong interactions [1–3]. As a way to quantify entanglement, one can bipartition a given system into two parts (A and B), and construct the reduced density matrix of A as $\rho_A = \mathrm{Tr}_B|\psi\rangle\langle\psi|$, using the ground state wave function $|\psi\rangle$. The entanglement entropy, $S = -\mathsf{Tr}(\rho_A \ln \rho_A)$, quantifies the amount of quantum entanglement between the halves, which has proved to be a profitable tool to explore quantum correlations encoded in ground state [4–7]. Following the seminal work Ref. [8], more recent developments have gone beyond the single number S, and invoked the full eigenvalue spectrum $\{p_n\}$ of ρ_A, dubbed as the entanglement spectra (ES). Nowadays, the ES has been treated as a more fine-grained "fingerprint" to distinguish various topological orders [8–11], symmetry protected phases [12, 13], symmetry broken phases [14, 15], quantum criticality [16–21], to name a few.

The reduced density matrix can be formally written as $\rho_A = e^{-H_E}$, and regarded as a thermal density matrix with entanglement Hamiltonian (EH) H_E at inverse temperature $\beta = 1$. Knowledge of the EH in terms of its operator content is of vital importance, because it could offer an alternative picture of how subsystem A behaves, by appealing to our intuition of thermodynamics. Moreover, the long-sought solution to some open questions actually relies on the access to the EH. For instance, a concrete form of the EH may provide insight for interesting problems such as bulk-edge correspondence [8, 22] and subsystem thermalization in the non-equilibrium dynamics [23–25]. From an information extraction point of view, both the entropy and the ES represent ways of reducing the full information content in ρ_A to more manageable forms. The analytical form of the EH, if achievable, points to a different reduction scheme, whereby the exponentially large complex-valued matrix elements in ρ_A are compressed into a handful of coupling constants in the EH.

Generally, it is technically challenging to work out the compact operator form of the EH, because the transformation $H_E = -\log \rho_A$ is non-linear. Only in a limited number of tractable cases, the EH can be explicitly obtained either exactly [26–29, 31] or perturbatively [32]. It has also been proposed to map out the EH through fitting the ES [15, 33], but it strongly depends on the empirical knowledge, and is thus uncontrolled. In addition, when putting on a lattice, the corrections to the field-theory predicted EH remains elusive [30]. Taken as a whole, despite these instructive attempts, to date there is no generic recipe to derive the EH in a compact form in strongly-correlated systems, thus a systematic scheme to directly access the EH is highly desired.

In this paper, to fill this gap, we present a systematic strategy to obtain the EH. Instead of evaluating $H_E = -\log \rho_A$ directly, we address this problem from an alternative angle, and propose to construct H_E based on the information of eigenstate of ρ_A. We demonstrate and benchmark this scheme on quantum spin lattice models. We confirm that, the obtained numerical EHs in these models converge to analytical forms, consistent with the corresponding conformal field theory (CFT) or perturbatively around exactly solvable points. Moreover, the method to quantify the accuracy of the obtained EH are also discussed through maximizing the density matrix fidelity. The present approach is not only applicable to a broad range of systems, but also opens a door to a variety of problems in condensed matter systems. For instance, the resulting EH bears an operator form similar to the corresponding physical Hamiltonian, which sheds some light on the understanding of Haldane's conjecture on entanglement spectra [8].

Method.— Our aim is to obtain the EH, $H_E = -\log \rho_A$, explicitly in terms of intelligible operators. This problem is in general analytically untractable due to the difficulty in evaluating the log. Below, we will instead (1) Confine ourselves to a restricted operator space $\mathcal{L}$ consisting of linear combinations of a prescribed set of basis operators, $\mathcal{L} = \mathrm{Span}\{L_a\}$, and then (2) Construct an operator $H_P \in \mathcal{L}$, such that it (approximately) shares one eigenstate with ρ_A (the entanglement ground state). In principle, H_P thus constructed may not be H_E, instead it could be a certain function of H_E. However, the EH obtained from the ground state of a local Hamiltonian is itself believed to be local. Thus as long as one chooses the operators $\{L_a\}$ properly (e.g. by including enough local operators), H_P and H_E should be equivalent up to a proper

rescale. We find this is indeed the case in the two examples to be discussed later.

To obtain H_P, we use a recently reported method [34–36] which takes as input a state $|\xi\rangle$ and a set of basis operators $\{L_a\}$, and returns a set of weights $\{w_a\}$, such that $H_P = \sum_a w_a L_a$ has $|\xi\rangle$ as an (approximate) eigenstate. Specifically, we take $|\xi\rangle$ as the entanglement ground state, and compute the correlation matrix

$$G_{ab} = \langle\xi|L_a L_b|\xi\rangle - \langle\xi|L_a|\xi\rangle\langle\xi|L_b|\xi\rangle \ . \tag{1}$$

Note that G is positive-semidefinite [37]. The desired weights are given by the eigenvector of the matrix G with the lowest eigenvalue $g_0 \geq 0$,

$$\{w_a\} : \sum_b G_{ab} w_b = g_0 w_a, \ g_0 = \min\{\mathsf{Spec}(G)\} \geq 0. \tag{2}$$

One can easily verify that $g_0 = \langle\xi|H_P^2|\xi\rangle - \langle\xi|H_P|\xi\rangle^2$, *i.e.*, g_0 is the "energy fluctuation" of the state $|\xi\rangle$ under "Hamiltonian" $H_P = \sum_a w_a L_a$. $|\xi\rangle$ becomes an exact eigenstate of H_P if $g_0 = 0$. For small but nonvanishing g_0, H_P is the best approximate parent "Hamiltonian" of $|\xi\rangle$ [38]. In practice, one can start with a small set of simple operators (e.g., 1- and short range 2-spin operators), and gradually add in more complicated ones (e.g., n-spin operators, longer range couplings, etc), until the calculated g_0 drops below a desired threshold value. When g_0 is small enough, the related eigenvector gives the local coupling strength in the EH. In this context, g_0, the fluctuation of the target state under the EH, serves the purpose of a control parameter, similar to the ground state energy in most variational calculation.

Although the above construction formally only ensures that H_P and H_E (approximately) share one eigenstate $|\xi\rangle$, we found in our study that the remainder of the eigenbasis also match well whenever g_0 is small, which we will quantify in the examples later. Note also that there is no *a priori* relation between the spectra of H_P and H_E even when the eigenbasis match exactly, this is why we take the more general form $H_P = f(H_E)$.

With H_P fixed, we can determine the best f, in principle, by maximizing the density matrix fidelity [39] between the original ρ_A and its reconstruction $\varrho = e^{-f(H_P)}$,

$$F(\rho_A, \varrho) = \mathsf{Tr}\sqrt{\sqrt{\rho_A}\varrho\sqrt{\rho_A}} \ . \tag{3}$$

We write the eigen-decomposition of ϱ as

$$\varrho(\boldsymbol{q}) = \sum_n q_n |\phi_n\rangle\langle\phi_n| \ , \tag{4}$$

where $\boldsymbol{q} = (q_1, q_2, \cdots)$, $q_n = e^{-f(\varepsilon_n)}$, and $|\phi_n\rangle$ and ε_n are the n^{th} eigenstate and eigenvalue of H_P, respectively. In Supple. Mater. [37], we show that maximizing $F(\rho_A, \varrho)$ leads to a self-consistent equation of $\boldsymbol{q}$. Its solution implicitly defines the f function through $f(\varepsilon_n) = -\log q_n$. When the eigenbasis $\{|\phi_n\rangle\}$ of H_P matches well with the entanglement states $\{|\xi_n\rangle\}$, the optimal $\boldsymbol{q}$ can be approximated by (see [37])

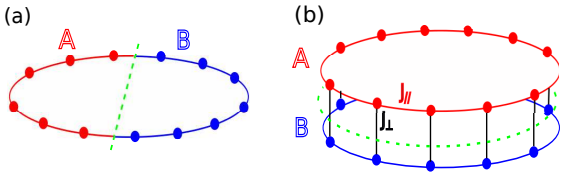

FIG. 1. (a) One-dimensional spin$-1/2$ chain and (b) spin ladder made of two coupled periodic spin$-1/2$ chain. The dashed line shows the entanglement bipartition into two subsystem A (red) and B (blue), each of which encloses L sites.

$$q_n \simeq \langle\phi_n|\rho_A|\phi_n\rangle \ \forall n \ . \tag{5}$$

Under this approximation, ϱ describes the diagonal ensemble of ρ_A in the reconstructed $\{|\phi_n\rangle\}$ basis.

Before going into examples, we remark that the EH can in principle be calculated by numerically evaluating $-\log\rho_A$ using exact diagonalization. Such calculations, however, require keeping track of the coefficients of exponentially many operators $|n\rangle\langle n'|$ in a many-body complete basis $\{|n\rangle\}$. Our method is numerically more efficient although it needs extra input regarding the physical properties of the system (reflected in the choice of $\{L_a\}$). More importantly, our method applies to situations (e.g. in simulations using matrix product state) where $\log\rho_A$ is hard to calculate numerically, as long as the correlation matrix remains tractable. As a nontrivial example, we demonstrate the quantum dynamics of equilibrated EH using time-dependent density matrix renormalization group (Ref. [37]).

One-dimensional chain.— As a first case example, we study the EH of bipartition of a one dimensional spin$-1/2$ chain model (as shown in Fig. 1(a)):

$$\hat{H} = \sum_{n=1}^{2L} \hat{h}_{n,n+1} = \sum_{n=1}^{2L} S_n^x S_{n+1}^x + S_n^y S_{n+1}^y + \Delta S_n^z S_{n+1}^z.$$

For $|\Delta| \leq 1$, the ground state can be effectively described by a gapless Luttinger liquid. By implementing the numerical scheme discussed in the method section, we search for a parent Hamiltonian with the form $H_P = \sum_n J_{n,n+1}\hat{h}_{n,n+1}$ on modest partition sizes. We analyze the salient features of the obtained EH. First of all, we identify one approximately zero eigenvalue in the spectrum of correlation matrix (Tab. I). The coefficients $J_{n,n+1}$ in H_P can be obtained from the corresponding eigenvector. Since subsystems A and B both have open boundaries after bipartition (Fig. 1(b)), translation symmetry is broken and $J_{n,n+1}$ is expected to be spatially dependent. In Fig. 2(a), we show the spatial dependence of $J_{n,n+1}$ (with proper normalization), where $J_{n,n+1}$ is non-uniform and takes smaller values near the virtual boundary. Importantly, for quantum critical phase of one dimensional spin$-1/2$ chain model, the EH is consequently expected to have the following conformal field theory (CFT)

TABLE I. Lowest eigenvalue g_0 of correlation matrix G, and density matrix fidelity $F(\rho_A, \varrho)$ obtained on different system sizes L for spin$-1/2$ Heisenberg chain ($\Delta = 1$).

$2 \times L$	20	24	28	32
g_0	3.9×10^{-8}	4.7×10^{-8}	4.4×10^{-8}	5.4×10^{-8}
$F(\rho_A, \varrho)$	0.99998	0.99998	0.99999	0.99997

form [23, 40–43]:

$$H_E^{\rm CFT} = \sum_{n=1}^{L-1} f_{\rm env}(\tilde{n}) \hat{h}_{n,n+1}, \tag{6}$$

where $f_{\rm env}(\tilde{n}) = \tilde{n}(1-\tilde{n})$ is the envelope function and $\tilde{n} = (n+\frac{1}{2})/L$. To elucidate the accuracy of our numerical method, we directly compare numerical results with the CFT prediction (Eq. 6). As shown in Fig. 2(a), the dependence of $J_{n,n+1}$ on n matches the CFT predicted envelope function $f_{\rm env}$ (black dashed line).

The agreement between $J_{n,n+1}$ and $f_{\rm env}(\tilde{n})$ suggests that for this model, H_P recovers H_E^{CFT}, and may indeed closely approximate the exact H_E. To verify, we first compare the ES $\{-\log p_n\}$ and the eigenvalues $\{\varepsilon_n\}$ of H_P [44]. As shown in Fig. 2(b), down to order 10^{-7}, the ES is extremely well captured by $\{\varepsilon_n\}$, evidenced by a simple linear fit $-\log p_n = a + b\varepsilon_n$. In addition, we compute the fidelity between the original and reconstructed reduced density matrix, $F(\rho_A, \varrho)$ where $\varrho = e^{-(a+bH_P)}$. As shown in Tab. I, $F(\rho_A, \varrho) > 0.9999$ for all system sizes tested. We thus conclude that H_P and H_E are indeed equivalent. Similar results are obtained throughout the gapless phase $|\Delta| \leq 1$ on all available system sizes. ($\Delta > 1$ case please see [37].)

Spin ladder model.— We turn to study a two-leg spin$-1/2$

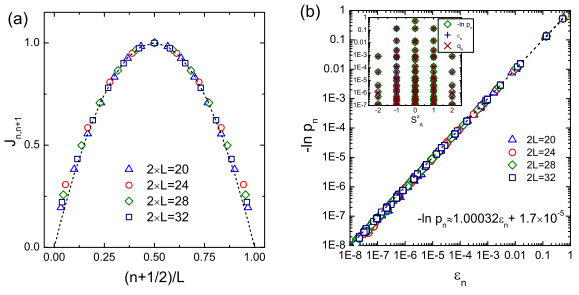

FIG. 2. (a) Spatially varying coupling strengths $J_{n,n+1}$ of the parent Hamiltonian of bipartition of a spin$-1/2$ Heisenberg chain. The black dashed lines show the CFT predicted envelope function $f_{\rm env}(\tilde{n}) = \tilde{n}(1-\tilde{n})$ and $\tilde{n} = \frac{n+(n+1)}{2L}$. (b) Direct comparison $-\log p_n$ of the ES, q_n by Eq. 41 and the eigenvalues ε_n of parent Hamiltonian H_P. The black line represents the best linear fit, with the slope ~ 1.00032 and intercept $\sim 10^{-5}$. Inset: One-to-one comparison of $-\log p_n$ of the ES and eigenvalues ε_n grouped by quantum number S_A^z in subsystem A. Different symbols show the results computed on $2 \times L$ systems: blue triangular ($L = 10$), red circles ($L = 12$), green diamonds ($L = 14$), navy squares ($L = 16$).

TABLE II. Parameters of H_E (Eq. 8) for $J_\perp/J_\parallel = 4$ and $\Delta = 1$ for spin ladder model.

$2L$	g_0	J_1	J_2	J_3	J_4
20	9.43×10^{-7}	0.9979	−0.0642	0.0041	−0.0024
24	6.96×10^{-6}	0.9979	−0.0646	0.0043	−0.0023
28	5.54×10^{-6}	0.9979	−0.0647	0.0039	−0.0023
32	4.80×10^{-6}	0.9979	−0.0637	0.0046	−0.0016

ladder Hamiltonian (as shown in Fig. 1(b)):

$$\begin{aligned}
\hat{H} &= \hat{H}_A + \hat{H}_B + \hat{H}_{AB} \\
\hat{H}_{\alpha=A(B)} &= J_\parallel \sum_{\langle ij \rangle} [S^x_{i,\alpha} S^x_{j,\alpha} + S^y_{i,\alpha} S^y_{j,\alpha} + \Delta S^z_{i,\alpha} S^z_{j,\alpha}] \\
\hat{H}_{AB} &= J_\perp \sum_i [S^x_{i,A} S^x_{i,B} + S^y_{i,A} S^y_{i,B} + \Delta S^z_{i,A} S^z_{i,B}],
\end{aligned} \tag{7}$$

where $J_\parallel = \cos\theta$ describes the nearest-neighbor exchange interaction in each chain, and $J_\perp = \sin\theta$ is "rung" exchange coupling between two chains. Below, we focus on the isotropic case $\Delta = 1$ and antiferromagnetic intra-chain coupling $J_\parallel > 0$ (see [37] for the anisotropic $\Delta > 1$). The nature of the ground state depends on the sign of $J_\perp$. For antiferromagnetic $J_\perp > 0$, spin singlets form on the rungs and the ground state can be viewed as the product of rung singles [45]. For ferromagnetic $J_\perp < 0$, the ladder system can be effectively mapped onto a spin-1 chain, thus the ground state is in the "Haldane" phase [46, 47].

We now reconstruct the EH H_E on chain A using translationally invariant Heisenberg couplings,

$$H_E = \sum_{n=1}^{N_r} J_n \hat{h}_n, \quad \hat{h}_n = \sum_{i=1}^{L} S_i \cdot S_{i+n}, \tag{8}$$

where $\hat{h}_n$ is the n-th neighbor coupling, and N_r is long-range interaction cut-off. As before, the coefficients J_n are obtained through diagonalization of correlation matrix G. We identify one *approximate* zero mode in the correlation spectrum. Tab. II shows one typical example of the corresponding coupling constants in the EH. First of all, we found that the reconstructed EH is dominated by the nearest-neighbor coupling, $J_1 \gg J_{n>1}$. Further-neighbor couplings decay as inter-spin distance increases, and we truncated at $N_r = 4^{th}$ neighbor coupling, which already yields very good reconstruction fidelity of $F(\rho_A, \varrho) > 0.998$. The vanishingly small long-ranged interactions reflects locality of the EH. We thus conclude that the main feature of the EH is captured by a spin$-1/2$ chain with nearest neighbor antiferromagnetic Heisenberg couplings. In addition, in Tab. II, we observe an unfrustrated ferromagnetic second-neighbor coupling $J_2 < 0$. The oscillatory nature of interaction couplings, which can be antiferromagnetic or ferromagnetic depending upon the separation, is reminiscent of the Ruderman-Kittel-Kasuya-Yosida interaction from which indirect interaction couplings in subsystem A can be induced through subsystem B.

To further understand the obtained EH, we make a perturbative calculation [37] in the strong inter-chain coupling limit ($J_\parallel \ll J_\perp$). Up to order $\mathcal{O}((\frac{J_\parallel}{J_\perp})^2)$,

$$H_E^{\rm per} \approx J_1^{\rm per} \sum_i S_i \cdot S_{i+1} - J_2^{\rm per} \sum_i S_i \cdot S_{i+2}, \quad (9)$$

where $J_1^{\rm per} = 2\frac{J_\parallel}{J_\perp}$ and $J_2^{\rm per} = \frac{1}{2}(\frac{J_\parallel}{J_\perp})^2$. Thus up to $\mathcal{O}(\frac{J_\parallel}{J_\perp})^2$, the EH behaves effectively as a spin$-1/2$ chain with first- and second-neighbor couplings. In particular, the second-neighbor coupling is ferromagnetic, consistent with our results in Tab. II. Fig. 3(b) shows quantitative agreement between perturbative and numerical results near $J_\parallel/J_\perp \to 0$, where numerics from different system sizes converge to the same perturbation theory values. This agreement not only provides an analytical understanding of the oscillatory nature of interaction couplings, but also validates the accuracy of our numerical results.

One major advantage of our current scheme is its applicability in the whole parameter regime, which is beyond the reach of perturbation-based effective theories. In Fig. 3(a), we show the EH parameters as a function of $\theta = \tan^{-1}(J_\perp/J_\parallel)$, up to fourth-neighbor couplings. At $\theta = 0$, the two chains are effectively decoupled, thus it is reasonable to obtain $J_{n>1}$ tending to zero. Away from this decoupling point, generally long-ranged interaction terms appear in H_E. We note that the obtained couplings J_n/J_1 show non-monotonic dependence on θ.

With the reconstructed EH in hand, a natural question is if it belongs in the same class with its physical counterpart $\hat{H}_A$. Since the ground state of H_E can be smoothly and adiabatically connected to that of $\hat{H}_A$ without gap closing (Fig. 3(c)), we conclude that H_E and $\hat{H}_A$ are indeed in the same class [48]. Interestingly, even though the whole system experiences a quantum phase transition at $\theta = 0$, the EH still faithfully represents the physical Hamiltonian $\hat{H}_A$.

Summary and Discussion.— We have presented a numerical scheme to reconstruct the entanglement Hamiltonian H_E based on entangled modes of reduced density matrix, with the help of the recently reported eigenstate-to-Hamiltonian mapping [34–36]. As a proof of principle, we applied this method to two quantum spin lattice models. We found that the reconstructed H_E accurately recovers the expected results and faithfully captures all features of the reduced density matrices, which are evidenced by direct comparison to analytical theories, the agreement between the original and reconstructed full entanglement spectra, and the close-to-1 density matrix fidelity.

This scalable recipe for constructing the entanglement Hamiltonian opens up a number of directions worthy of further exploration. We explicitly showed in our examples that H_E bears a similar form as the physical Hamiltonian, which unambiguously supports the conjecture that there exists a deep correspondence between the entanglement Hamiltonian and the physical Hamiltonian with a virtual boundary [8, 22, 49]. Similar numerical calculations may be used to investigate the time evolution of entanglement Hamiltonian [23–25], which may provide intuitive pictures and additional insights regarding the nature of entanglement propagation and subsystem thermalization; see supplemental materials Ref. [37] for the extraction of equilibrated entanglement Hamiltonian after a quantum quench. This work also paves the way for future studies of entanglement Hamiltonian in higher dimensions using matrix product state and similar variational ansatz, for which the correlation matrix (Eq. 1) remains accessible at moderate system sizes.

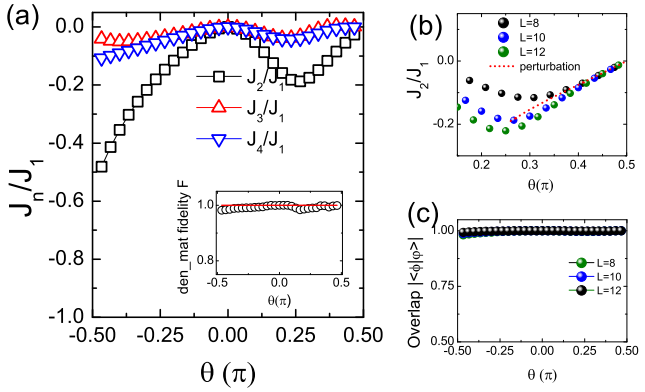

FIG. 3. (a) EH parameters J_n/J_1 versus θ (up to fourth nearest neighbor) for a given size $L = 12$. Inset: Density matrix fidelity $F(\rho_A, \varrho)$ between ρ_A and ϱ versus θ. (b) Comparison EH parameters J_2/J_1 and the perturbation theory Eq. 9 (red dashed line). Different symbols stand for $L = 8$ (green), $L = 10$ (blue), $L = 12$ (black). $\theta \to \pi/2$ relates to the strong inter-chain coupling limit. (c) Wave function fidelity $|\langle\phi_E^0|\varphi_A^0\rangle|$ as a function of θ, where $|\varphi_A^0\rangle$ and $|\phi_E^0\rangle$ is the ground state of $\hat{H}_A$ and H_E, respectively.

Note added.— At the final stage of preparing this manuscript, we became aware of a different scheme to map out entanglement Hamiltonian [50]. Applications of similar numerical schemes to related problems have been reported in [52, 53] shortly after the initial submission of this work.

Acknowledgments.— We thank Y. Zhang, D. N. Sheng, Xueda Wen, J.X-.Zhu, D.P. Arovas for fruitful discussion. This work was supported by U.S. DOE at Los Alamos National Laboratory (W.Z., Z.S.H.). Y.C.H. was supported by the Gordon and Betty Moore Foundation under the EPiQS initiative, GBMF4306, at Harvard University. This research was also supported in part by Perimeter Institute for Theoretical Physics (Y.C.H.). Research at Perimeter Institute is supported by the Government of Canada through the Department of Innovation, Science and Economic Development Canada and by the Province of Ontario through the Ministry of Research, Innovation and Science.

[1] L. Amico, R. Fazio, A. Osterloh, and V. Vedral, Rev. Mod. Phys. **80**, 517 (2008), URL http://link.aps.org/doi/10.1103/RevModPhys.80.517.

[2] N. Laflorencie, Physics Reports **646**, 1 (2016), ISSN 0370-1573, quantum entanglement in condensed matter systems, URL http://www.sciencedirect.com/science/article/pii/S0370157316301582.

[3] J. Eisert, M. Cramer, and M. B. Plenio, Rev. Mod. Phys. **82**, 277 (2010), URL http://link.aps.org/doi/10.1103/RevModPhys.82.277.

[4] G. Vidal, J. I. Latorre, E. Rico, and A. Kitaev, Phys. Rev. Lett. **90**, 227902 (2003), URL https://link.aps.org/doi/10.1103/PhysRevLett.90.227902.

[5] P. Calabrese and J. Cardy, Journal of Statistical Mechanics: Theory and Experiment **2004**, P06002 (2004).

[6] A. Kitaev and J. Preskill, Phys. Rev. Lett. **96**, 110404 (2006), URL http://link.aps.org/doi/10.1103/PhysRevLett.96.110404.

[7] M. Levin and X.-G. Wen, Phys. Rev. Lett. **96**, 110405 (2006), URL http://link.aps.org/doi/10.1103/PhysRevLett.96.110405.

[8] H. Li and F. D. M. Haldane, Phys. Rev. Lett. **101**, 010504 (2008), URL http://link.aps.org/doi/10.1103/PhysRevLett.101.010504.

[9] A. M. Läuchli, E. J. Bergholtz, J. Suorsa, and M. Haque, Phys. Rev. Lett. **104**, 156404 (2010), URL http://link.aps.org/doi/10.1103/PhysRevLett.104.156404.

[10] L. Cincio and G. Vidal, Phys. Rev. Lett. **110**, 067208 (2013), URL http://link.aps.org/doi/10.1103/PhysRevLett.110.067208.

[11] M. P. Zaletel, R. S. K. Mong, and F. Pollmann, Phys. Rev. Lett. **110**, 236801 (2013), URL http://link.aps.org/doi/10.1103/PhysRevLett.110.236801.

[12] F. Pollmann, A. M. Turner, E. Berg, and M. Oshikawa, Phys. Rev. B **81**, 064439 (2010), URL http://link.aps.org/doi/10.1103/PhysRevB.81.064439.

[13] F. Pollmann, E. Berg, A. M. Turner, and M. Oshikawa, Phys. Rev. B **85**, 075125 (2012), URL http://link.aps.org/doi/10.1103/PhysRevB.85.075125.

[14] M. A. Metlitski and T. Grover, ArXiv e-prints (2011), 1112.5166.

[15] V. Alba, M. Haque, and A. M. Läuchli, Phys. Rev. Lett. **110**, 260403 (2013), URL https://link.aps.org/doi/10.1103/PhysRevLett.110.260403.

[16] G. De Chiara, L. Lepori, M. Lewenstein, and A. Sanpera, Phys. Rev. Lett. **109**, 237208 (2012), URL https://link.aps.org/doi/10.1103/PhysRevLett.109.237208.

[17] D. Poilblanc, Phys. Rev. Lett. **105**, 077202 (2010).

[18] J. I. Cirac, D. Poilblanc, N. Schuch, and F. Verstraete, Phys. Rev. B **83**, 245134 (2011), URL https://link.aps.org/doi/10.1103/PhysRevB.83.245134.

[19] T. H. Hsieh and L. Fu, Phys. Rev. Lett. **113**, 106801 (2014), URL http://link.aps.org/doi/10.1103/PhysRevLett.113.106801.

[20] A. Bayat, H. Johannesson, S. Bose, and P. Sodano, Nat. Comm. **5**, 3784 (2014).

[21] I. Frérot and T. Roscilde, Phys. Rev. Lett. **116**, 190401 (2016), URL https://link.aps.org/doi/10.1103/PhysRevLett.116.190401.

[22] X.-L. Qi, H. Katsura, and A. W. W. Ludwig, Phys. Rev. Lett. **108**, 196402 (2012), URL http://link.aps.org/doi/10.1103/PhysRevLett.108.196402.

[23] J. Cardy and E. Tonni, Journal of Statistical Mechanics: Theory and Experiment **12**, 123103 (2016), 1608.01283.

[24] P. Calabrese and J. Cardy, Journal of Statistical Mechanics: Theory and Experiment **2005**, P04010 (2005), URL http://stacks.iop.org/1742-5468/2005/i=04/a=P04010.

[25] Xueda Wen, Shinsei Ryu, Andreas W. W. Ludwig, arXiv.1807.04440.

[26] M.-C. Chung and I. Peschel, Phys. Rev. B **62**, 4191 (2000), URL https://link.aps.org/doi/10.1103/PhysRevB.62.4191.

[27] I. Peschel, Journal of Physics A: Mathematical and General **36**, L205 (2003), URL http://stacks.iop.org/0305-4470/36/i=14/a=101.

[28] L. Fidkowski, Phys. Rev. Lett. **104**, 130502 (2010), URL http://link.aps.org/doi/10.1103/PhysRevLett.104.130502.

[29] I. Klich, D. Vaman, and G. Wong, Phys. Rev. Lett. **119**, 120401 (2017), URL https://link.aps.org/doi/10.1103/PhysRevLett.119.120401.

[30] V. Eisler and I. Peschel, ArXiv e-prints (2018), 1805.00078.

[31] B. Nienhuis, M. Campostrini, and P. Calabrese, Journal of Statistical Mechanics: Theory and Experiment **2009**, P02063 (2009), URL http://stacks.iop.org/1742-5468/2009/i=02/a=P02063.

[32] A. M. Läuchli and J. Schliemann, Phys. Rev. B **85**, 054403 (2012), URL https://link.aps.org/doi/10.1103/PhysRevB.85.054403.

[33] Hiroyuki Fujita, Yuya O. Nakagawa, Sho Sugiura, and Masaki Oshikawa Phys. Rev. B 97, 075114 (2018).

[34] X.-L. Qi and D. Ranard, ArXiv e-prints (2017), 1712.01850.

[35] E. Chertkov and B. K. Clark, ArXiv e-prints (2018), 1802.01590.

[36] M. Greiter, V. Schnells, and R. Thomale, ArXiv e-prints (2018), 1802.07827.

[37] Supplementary Materials .

[38] It is the best in the sense that if the basis operators $\{L_a\}$ are orthonormal (that is, $\mathsf{Tr}(L_a^\dagger L_b) = \delta_{ab}\mathsf{Tr}\mathbb{I}$, where $\mathbb{I}$ is the identity), and if $\sum_a |w_a|^2 = 1$ is also normalized, then out of all *normalized* operators $\{H \in \mathcal{L} | \mathsf{Tr}(H^\dagger H) = \mathsf{Tr}\mathbb{I}\}$, H_P has the smallest fluctuation with respect to the given state $|\xi\rangle$. See [37] for more details.

[39] A. Uhlmann, Reports on Mathematical Physics **9**, 273 (1976).

[40] J. Bisognano and E. H. Wichmann, Jour. Math. Phys. **16**, 985 (1975), URL https://doi.org/10.1063/1.522605.

[41] J. Bisognano and E. H. Wichmann, Jour. Math. Phys. **17**, 303 (1976), URL https://doi.org/10.1063/1.522898.

[42] H. Casini, M. Huerta, and R. C. Myers, Journal of High Energy Physics **5**, 36 (2011), 1102.0440.

[43] X. Wen, S. Ryu, and A. W. W. Ludwig, Phys. Rev. B **93**, 235119 (2016), URL https://link.aps.org/doi/10.1103/PhysRevB.93.235119.

[44] The proper renormalization of eigenvalues $\{\varepsilon_n\}$ of H_P is need to satisfy the condition $\sum_n e^{-\varepsilon_n} = 1$.

[45] T. Barnes, E. Dagotto, J. Riera, and E. S. Swanson, Phys. Rev. B **47**, 3196 (1993).

[46] F. Haldane, Physics Letters A **93**, 464 (1983), ISSN 0375-9601.

[47] S. P. Strong and A. J. Millis, Phys. Rev. Lett. **69**, 2419 (1992).

[48] Here, we use the definition that two Hamiltonians are in the same class, if they can be smoothly connected through a family of Hamiltonians.

[49] M. Dalmonte, B. Vermersch and P. Zoller, Nat. Phys. 14, 827 (2018).

[50] Parisen Toldin, F. Assaad, Phys. Rev. Lett. 121, 200602 (2018).

[51] H.-J. Mikeska and A. K. Kolezhuk, *One-dimensional magnetism* (Springer Berlin Heidelberg, Berlin, Heidelberg, 2004), pp. 1–83, ISBN 978-3-540-40066-0, URL https://doi.org/10.1007/BFb0119591.

[52] E. Bairey, I. Arad, and N. H. Lindner, Phys. Rev. Lett. 122, 020504 (2019).

[53] X. Turkeshi, T. Mendes-Santos, G. Giudici, M. Dalmonte, Phys. Rev. Lett. 122, 150606 (2019).

I. CONSTRUCTING A PARENT OPERATOR FROM AN EIGENSTATE, A LINEAR DEPENDENCY PERSPECTIVE

In Ref. 34 (see also Refs. 35 and 36), Qi and Ranard showed that given a manybody wavefunction $|v\rangle$, a (more or less) unique parent Hamiltonian can be constructed in the form

$$H = \sum_i w_i L_i \ , \tag{10}$$

where $\{L_i\}$ is a set of Hermitian operators, if and only if the following "correlation matrix" $M_{ij}^{(v)}$ has a unique zero eigenvalue (with eigenvector $(w_1, w_2, \cdots)$),

$$M_{ij}^{(v)} \equiv \frac{1}{2}\langle v|\{L_i \ , \ L_j\}|v\rangle - \langle v|L_i|v\rangle\langle v|L_j|v\rangle \ , \tag{11}$$

$$\sum_j M_{ij}^{(v)} w_j \stackrel{!}{=} 0 \ . \tag{12}$$

Restricting $\{L_i\}$ to spatially local operators, the above observation then provides a guiding principle for constructing a local parent Hamiltonian for an arbitrary state $|v\rangle$. Note that $|v\rangle$ is not necessarily the ground state of thus constructed H.

We now provide an alternative perspective for the above and other related results, in terms of a linear dependence analysis. A *sufficient and necessary* condition for a normalized state $|v\rangle$ to be an eigenstate of H is that

$$(\mathbb{I} - P_v)H|v\rangle = 0 \quad , \quad P_v \equiv |v\rangle\langle v| \ , \tag{13}$$

where $\mathbb{I}$ is identity, and P_v projects onto $|v\rangle$. Consider now a Hamiltonian of the form Eq. 10. Then

$$(\mathbb{I} - P_v)H|v\rangle = \sum_i w_i |u_i\rangle \quad , \quad |u_i\rangle \equiv (\mathbb{I} - P_v)L_i|v\rangle \ . \tag{14}$$

The unnormalized $\{|u_i\rangle\}$ states are generated by first "exciting" $|v\rangle$ by L_i, and then projecting out the part parallel to $|v\rangle$. Eq. 13 is equivalent to demanding that the $\{|u_i\rangle\}$ states are *linearly dependent*,

$$\sum_i w_i |u_i\rangle = 0 \ . \tag{15}$$

Linear dependence of a set of vectors can be checked via a principal component analysis, which is mathematically equivalent to a singular value decomposition (SVD). To proceed, we construct a $D \times M$ matrix A by arranging $|u_i\rangle$ as its i^{th} column,

$$A_{D\times M} \equiv (|u_1\rangle \ , \ |u_2\rangle \ , \ \cdots) \ . \tag{16}$$

Here D is the full Hilbert space dimension, and M is the rank of the operator set $\{L_a\}$, $a = 1, 2, \cdots, M$. The linear dependence condition Eq. 15 is formally equivalent to demanding that A has at least one zero *singular* value (a more detailed discussion of the related SVD will be provided below). Equivalently, the overlap matrix $G_{ij} = (A^\dagger A)_{ij} = \langle u_i|u_j\rangle$ should have at least one zero *eigenvalue*, with the coefficients $\{w_i\}$ given by the corresponding eigenvector,

$$G_{ij} = \langle u_i|u_j\rangle = \langle v|L_i L_j|v\rangle - \langle v|L_i|v\rangle\langle v|L_j|v\rangle \ , \tag{17}$$

$$\sum_j G_{ij} w_j \stackrel{!}{=} 0 \ . \tag{18}$$

Note that Qi and Ranard's correlation matrix M is the real part of the hermitian G matrix. Replacing G with M is equivalent to enforcing real-valuedness of the resulting coefficients $\{w_i\}$, as required by the Hermiticity of $H = \sum w_i L_i$. A non-Hermitian parent operator H can be viewed as an annihilator of the state $|v\rangle$, as discussed in Ref. 36

1. Principal component analysis of the states $\{L_i|v\rangle\}$

In practice, the choice of the basis operators $\{L_i\}$ is often based on physical intuition, so for efficiency reasons one may start with a relatively small set of $\{L_i\}$, and gradually add in more operators (e.g., in increasing order of spatial span or other physical

preferences), until the lowest singular value of A (or eigenvalue of $G = A^\dagger A$) converges toward zero. A natural question therefore concerns the meaning of the SVD of A, which we now address. The SVD reads

$$A_{D\times M} = \mathsf{L}\Lambda\mathsf{R}^\dagger = \sum_{i=1}^{M} \lambda_i |l_i\rangle\langle r_i| \quad , \quad \Lambda = \mathsf{Diag}(\lambda_1, \lambda_2, \cdots, \lambda_M) \, , \tag{19}$$

$$\mathsf{L}_{D\times M} = (|l_1\rangle, |l_2\rangle, \cdots, l_M\rangle) \quad , \quad \mathsf{R}_{M\times M} = (|r_1\rangle, |r_2\rangle, \cdots, |r_M\rangle \, . \tag{20}$$

The columns of L and R are the left and right singular vectors, respectively, and are denoted as $|l_i\rangle$ and $|r_i\rangle$. Note that the right singular vectors (which are the eigenvectors of G) are M-dimensional. Vectors in the right singular space Span$\{|r_i\rangle\}$ represent operators in the operator space Span$\{L_i\}$: Writing the i^{th} right singular vector as

$$|r_i\rangle = (r_i^{(1)}, r_i^{(2)}, \cdots, r_i^{(M)})^t \, , \tag{21}$$

then the corresponding "Hamiltonian" is

$$H^{(i)} \equiv \sum_j L_j r_i^{(j)} = (L_1, L_2, \cdots, L_M)|r_i\rangle \, , \tag{22}$$

similar in spirit to writing polarized spin operators as $\sigma_{\boldsymbol{b}} = \boldsymbol{b}\cdot\boldsymbol{\sigma}$. One can then verify that

$$(\mathbb{I} - P_v)H^{(i)}|v\rangle = A|r_i\rangle = \lambda_i|l_i\rangle \, . \tag{23}$$

The first equality follows from Eq. 16, and the second one follows from Eq. 19. Note that $\langle v|l_i\rangle = 0 \forall i$, which can be checked by left multiplying $\langle v|$ to the above equation. In words, this equation means that the action of $H^{(i)}$ on $|v\rangle$ generates a deviation, perpendicular to $|v\rangle$, as given by the corresponding left singular vector $|l_i\rangle$, with weight λ_i (the singular value). In particular, if $\lambda_i = 0$, then one recovers Eq. 13, and $|v\rangle$ becomes an eigenstate of $H^{(i)}$. Thinking of $H^{(i)} = i\partial_t$ as a time evolution generator, then the LHS is the *covariant* time derivative iD_t. The i^{th} left singular vector $|l_i\rangle$ is thus the normalized tangent vector generated by $H^{(i)}$, and the corresponding singular value is related to the Fubini-Study metric in the time direction, $\lambda_i^2 = \langle v|D_t^2|v\rangle$, which is also the energy fluctuation,

$$\lambda_i^2 = \langle v|H^{(i)}(\mathbb{I} - P_v)H^{(i)}|v\rangle = \langle {H^{(i)}}^2\rangle_v - \langle H^{(i)}\rangle_v^2 \, . \tag{24}$$

2. In what sense is the reconstructed parent operator optimal?

The right singular vectors satisfy orthonormality $\langle r_i|r_j\rangle = \delta_{ij}$. What does it entail for their operator counterparts $H^{(i)}$ (Eq. 22)? In order to carry this over to the operator space, one should additionally require the operators $\{L_i\}$ to satisfy certain operator orthonormality, which, up until now, we have not enforced. Following Qi and Ranard [34], we use the Hilbert-Schmidt inner product for operators,

$$\langle A, B\rangle \equiv \frac{1}{\mathsf{Tr}\mathbb{I}}\mathsf{Tr}(A^\dagger B) \, , \tag{25}$$

where $\mathsf{Tr}\mathbb{I} = D$ is the full Hilbert space dimension. An orthonormal *operator* basis $\{L_i\}$ satisfies

$$\langle L_i, L_j\rangle \stackrel{!}{=} \delta_{ij}. \tag{26}$$

Then "Hamiltonians" corresponding to different right singular vectors also satisfy orthonormality,

$$\langle H^{(i)}, H^{(j)}\rangle = \sum_{i',j'} r_i^{(i')} r_j^{(j')} \langle L^{(i')}, L^{(j')}\rangle = \langle r_i|r_j\rangle = \delta_{ij} \, . \tag{27}$$

In other words, these "eigen-Hamiltonians" $\{H^{(i)}\}$ form an orthonormal basis for the operator space spanned by $\{L_i\}$. A normalized *traceless* "Hamiltonian" H simply means its spectrum has unit variance, $\mathsf{Tr}(H^2)/\mathsf{Tr}(\mathbb{I}) \stackrel{!}{=} 1$.

Using orthonormal $\{L_i\}$, then in situations where an exact zero eigenvalue does not exist for G (Eq. 17), the parent operator $H^{(i_{min})}$ corresponding to the lowest eigenvalue of G is an "optimal" approximate parent Hamiltonian, in the sense that out of all *normalized* operators in the space of Span$\{L_i\}$, $H^{(i_{min})}$ generates the lowest energy fluctuation on $|v\rangle$, or equivalently the least deviation of $H|v\rangle$ from $|v\rangle$.

II. QUANTIFYING THE QUALITY OF THE RECONSTRUCTED BASIS USING IPR

The method described in the text is based on the ansatz that the reduced density matrix (RDM) ρ_A can be written as a scalar function y of a local operator H_P, and H_P itself is to be (approximately) constructed, from an exact eigenstate $|\xi\rangle$ of ρ_A, in the space of $\mathcal{L} \equiv \text{Span}\{L_i\}$,

$$\rho_A \stackrel{?}{=} y(H_P) \quad , \quad H_P \in \mathcal{L} \, . \tag{28}$$

The construction scheme for H_P, however, only guarantees that H_P and ρ_A (approximately) share one eigenstate $|\xi\rangle$, with no constraint on the remainder of the eigenbasis. Therefore, to claim that one has successfully reconstructed ρ_A in terms of $\{L_i\}$, one needs to verify that the entire eigenbasis of H_P approximately matches that of ρ_A.

A simple way to quantify the quality of one set of basis states $\{|\phi_n\rangle\}$ in terms of their similarity to a reference basis $\Psi \equiv \{|\psi_n\rangle\}$, is to use the inverse participation ratio,

$$\text{IPR}(\phi_n|\Psi) = \frac{1}{\sum_{m=1}^{N} |\langle\phi_n|\psi_m\rangle|^4} \in [1, N] \, . \tag{29}$$

The IPR measures effectively how many basis states in Ψ one needs to span a particular $|\phi_n\rangle$. It is 1 if $\langle\phi_n|\psi_m\rangle = \delta_{m,n}$, and saturates to N if $|\langle\phi_n|\psi_m\rangle| = \frac{1}{\sqrt{N}}\ \forall m$. In the context of RDM reconstruction, one would compute the IPR for each of the eigenstates of H_P in the exact eigenbasis of ρ_A; if all of them are close to 1, then H_P and ρ_A approximately share the same set of basis states.

1. Generalized IPR in the presence of degeneracy

When H_P has degeneracy, there is a $U(M)$ indeterminacy in an M-fold degenerate subspace $\mathcal{M}$. Then taking a single numerically obtained eigenstate out of this M-dimensional subspace may yield a "broadened" IPR (i.e., one > 1), even if upon a $U(M)$ transformation, each of the M (transformed) states could have a perfectly sharp IPR (i.e., $= 1$). To fix this, we generalize the notion of IPR to a degenerate subspace. Denote the projection operator of this subspace and a corresponding density operator as

$$P_{\mathcal{M}} = \sum_{n=n_1}^{n_M} |\phi_n\rangle\langle\phi_n| \quad , \quad \rho_{\mathcal{M}} = P_{\mathcal{M}}/\mathsf{Tr}P_{\mathcal{M}} \, . \tag{30}$$

The generalized IPR is defined as the exponentiated 2^{nd} Renyi entropy, e^{S_2}, of the diagonal ensemble in the Ψ basis,

$$\text{IPR}(P_{\mathcal{M}}|\Psi) = \frac{1}{\sum_{m=1}^{N} \langle\psi_m|\rho_{\mathcal{M}}|\psi_m\rangle^2} \, . \tag{31}$$

One can verify that the generalized IPR reduces to the standard one when there is no degeneracy ($M \to 1$). Note that if $P_{\mathcal{M}}$ exactly matches an equal-dimensional subspace in the Ψ basis, $P_{\mathcal{M}} = \sum_{n=n_1}^{n_M} |\psi_n\rangle\langle\psi_n|$, then $\langle\psi_m|\rho_{\mathcal{M}}|\psi_m\rangle = \frac{1}{M}$, hence $\text{IPR}(P_{\mathcal{M}}|\Psi) = M$. In other words, in the perfect match case, the generalized IPR is given by the dimension of the degenerate subspace $\mathcal{M}$. On the other hand, if each of the degenerate $|\phi_{n_i}\rangle$ still satisfies $|\langle\phi_{n_i}|\psi_m\rangle| = \frac{1}{\sqrt{N}}\forall m$, then $\langle\psi_m|\rho_{\mathcal{M}}|\psi_m\rangle = \frac{1}{N}$, hence IPR $= N$. The generalized IPR thus reflects the notion of effective number of $|\psi\rangle$ states needed to span the subspace $P_{\mathcal{M}}$.

2. Direct comparison the eigenstates of entanglement Hamiltonian and those of parent Hamiltonian using IPR

In this section, we explicitly show the comparison of eigenstates of H_P with those of H_E using IPR. We take the 1D spin chain as example again. Since the reconstructed H_E has degeneracy, we use the generalized IPR introduced in Eq. 31 when appropriate. In Fig. 4(a-b) we repeat the same scheme as in the main text and compare the eigenvalues of H_P and H_E. In Fig. 4(c), we show the IPR of eigenstates of H_P as labeled by their (renormalied) weight ε_n. It is found $IPR_n \approx 1$ for all of eigenstates with weight $\varepsilon_n > 10^{-6}$, showing that each eigenstate of H_E is identical to the eigenstate of H_P. Please note that, for worst case, if the eigenstates of H_P and that of H_E are totally independent, it should be expected maximum value of $IPR \sim N \sim 2^{L/2}$ (L total system size) which is exponential growing with L. In Fig. 4(c), IPR_n are all close to 1 show that the eigenstates of H_P has well captured the eigenstates of H_E.

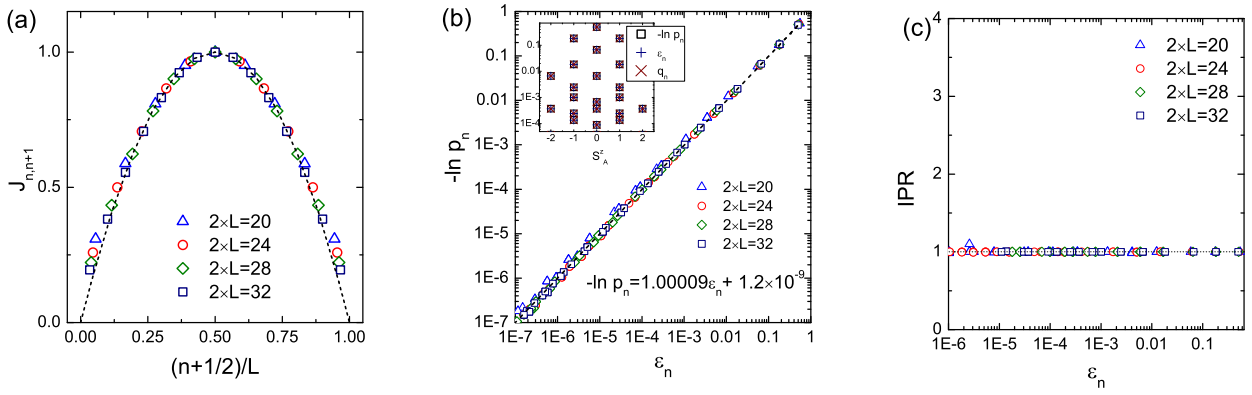

FIG. 4. (a) Spatially varying coupling strengths $J_{n,n+1}$ of the parent Hamiltonian of bipartition of a one-dimension spin$-1/2$ chain model at XY point ($\Delta = 0$). The black dashed lines show the CFT predicted envelope function $f_{\rm env}(\tilde{n}) = \tilde{n}(1-\tilde{n})$ and $\tilde{n} = \frac{n+(n+1)}{2L}$. (b) Direct comparison $-\log p_n$ of the ES, q_n by Eq. 41 and the eigenvalues ε_n of parent Hamiltonian H_P. The black line represents the best linear fit, with the slope ~ 1.000090 and intercept $\sim 10^{-9}$. Inset: One-to-one comparison of $-\log p_n$ of the ES and eigenvalues ε_n grouped by quantum number S^z_A in subsystem A. (c)Inverse participation ratio of eigenstates of parent Hamiltonian H_P. Different symbols show the results computed on $2 \times L$ systems: blue triangular ($L = 10$), red circles ($L = 12$), green diamonds ($L = 14$), navy squares ($L = 16$).

In the main text, we have demonstrated that the eigenvalue of parent Hamiltonian H_P has one-to-one correspondence with the entanglement spectra of reduced density matrix. Here, we further show that each eigenstate of H_P can be captured by the eigenstate of H_E. Taking into account that density matrix fidelity $F(\rho_A, \varrho) = \mathsf{Tr}\sqrt{\sqrt{\rho_A}\varrho\sqrt{\rho_A}}$ itself reveals the weighted averaged wavefunction overlap between the eigenstates of H_P and that of H_E, we now can understand very large value of density matrix fidelity as shown in the main text. In conclusion, the very large density matrix fidelity unambiguously sets up the equivalence between H_P and entanglement Hamiltonian H_E.

In Fig. 4 and Tab. III, we show the results at parameter $\Delta = 0$ of spin chain model (Fig. 1(a) in main text). The reason for this choice is two-fold. First, complementary to the Heisenberg point $\Delta = 1$ which has been shown in the main text, the results at XY point $\Delta = 0$ provide additional evidences, supporting the EH are similar in the whole critical spin liquid regime $|\Delta| \leq 1$. Second, the XY point is analytic solvable through Wigner-Jordan transformation. Compared with the existing results [30], the obtaining H_E faithfully represents the dominant, conformal part of the exact entanglement Hamiltonian.

III. OPTIMIZING REDUCED DENSITY MATRIX RECONSTRUCTION FIDELITY

Under the ansatz Eq. 28, if the eigenbasis of the constructed H_P matches exactly with that of the target RDM ρ_A, then the scalar function y is implicitly determined through the map between their spectra, $y(\varepsilon_n) = p_n$, where ε_n and p_n are the eigenvalue of H_P and ρ_A, respectively, associated with their common eigenvector $|\psi_n\rangle$. When the basis reconstruction is only approximate, the best y function can be determined in principle by maximizing the fidelity between the original and reconstructed RDMs. For clarity, in this section we will drop the subscript $_A$ and denote the target RDM as ρ. Its eigen decomposition is

$$\rho = \sum_n p_n |\psi_n\rangle\langle\psi_n| \,. \tag{32}$$

TABLE III. Lowest eigenvalue g_0 of correlation matrix G, and density matrix fidelity $F(\rho_A, \varrho)$ obtained on different system sizes L. Here we set $\Delta = 0$ in one-dimension spin$-1/2$ chain model.

$2 \times L$	20	24	28	32
g_0	2.9×10^{-14}	1.4×10^{-13}	1.2×10^{-13}	9.4×10^{-15}
$F(\rho_A, \varrho)$	0.99999	0.99998	0.99996	0.99991

The reconstructed density matrix is $\varrho = y(H_P)$ with as of yet unknown y, where $H_P = \sum_n \varepsilon_n |\phi_n\rangle\langle\phi_n|$ is the reconstructed parent operator. The eigen decomposition of ϱ is therefore

$$\varrho = \sum_n q_n |\phi_n\rangle\langle\phi_n| \,, \tag{33}$$

where $q_n = y(\varepsilon_n)$. The fidelity between the original and the reconstructed RDMs is defined as

$$F(\rho,\varrho) = \mathsf{Tr}\hat{F}(\rho,\varrho) \quad , \quad \hat{F}(\rho,\varrho) \equiv \sqrt{\sqrt{\rho}\,\varrho\sqrt{\rho}}\,. \tag{34}$$

It will be useful to note that the operator $\hat{F}(\rho,\varrho)$ arises from the following *polar decomposition*,

$$\sqrt{\rho_1}\sqrt{\rho_2} = \hat{F}(\rho_1,\rho_2)U(\rho_1,\rho_2) \quad , \quad U(\rho_1,\rho_2)^\dagger = U(\rho_2,\rho_1)\,, \tag{35}$$

where the unitary $U(\rho_1,\rho_2)$, although not of our concern in the present context, is related to Uhlmann's parallel transport of density matrices [39], and the second equation follows from the hermiticity of $\hat{F}(\rho_1,\rho_2)$. The maximization of F can be viewed as a variational problem in the space of normalized distributions $\{q_n\}$, and once the optimal weights are obtained, y can be determined (or defined) through $y(\varepsilon_n) = q_n$.

The stationary condition for extremal F over the variational space of $\{q_n\}$ is

$$\frac{\partial}{\partial q_n}\Big[F - \lambda(\sum_m q_m - 1)\Big] = 0\,, \tag{36}$$

where λ is the Lagrangian multiplier for the normalization $\sum_m q_m = 1$. Using $\partial\mathsf{Tr}\sqrt{A} = \frac{1}{2}\mathsf{Tr}(\sqrt{A}^{-1}\partial A)$ for any invertible operator A, Eq. 36 becomes

$$\frac{\partial F}{\partial q_n} = \frac{1}{2}\langle\phi_n|\hat{Q}|\phi_n\rangle = \lambda \quad \forall n\,, \tag{37}$$

where $\hat{Q} = \sqrt{\rho}\hat{F}(\rho,\varrho)^{-1}\sqrt{\rho}$. Using Eq. 35, one can show that $\hat{F}(\rho,\varrho)^{-1} = U(\rho,\varrho)\sqrt{\varrho}^{-1}\sqrt{\rho}^{-1}$, thus

$$\hat{Q} = \sqrt{\varrho}^{-1}\hat{F}(\varrho,\rho)\sqrt{\varrho}^{-1}\,, \tag{38}$$

and Eq. 37 becomes $\langle\phi_n|\hat{F}(\varrho,\rho)|\phi_n\rangle = 2\lambda q_n\,\forall n$. Note that $\sum_n q_n = 1$, thus $2\lambda = \sum_n LHS = \mathsf{Tr}\hat{F}(\varrho,\rho) = F(\varrho,\rho)$, and we finally arrive at a self consistent equation for the weights $\{q_n\}$,

$$\frac{\langle\phi_n|\hat{F}(\varrho,\rho)|\phi_n\rangle}{\sum_n\langle\phi_n|\hat{F}(\varrho,\rho)|\phi_n\rangle} = q_n \quad \forall n\,, \tag{39}$$

note that the LHS depends on $\{q_n\}$ only through ϱ.

1. Approximate optimal solution in the high-fidelity limit

When the two bases $\{|\psi\rangle\}$ and $\{|\phi\rangle\}$ have a good match, the fidelity operator $\hat{F}$ (Eq. 34) is dominated by its diagonal line (say, in the $\{|\phi\rangle\}$ basis). In this case one may adopt the approximation that

$$\langle\phi_n|\sqrt{\hat{F}^2(\varrho,\rho)}|\phi_n\rangle \simeq \sqrt{\langle\phi_n|\hat{F}^2(\varrho,\rho)|\phi_n\rangle} = \sqrt{q_n}\sqrt{\langle\phi_n|\rho|\phi_n\rangle}\,. \tag{40}$$

Substituting this into Eq. 39, one then obtains

$$q_n \simeq \langle\phi_n|\rho|\phi_n\rangle\,, \tag{41}$$

that is, the optimal q_n is the weight of the reconstructed eigenstate $|\phi_n\rangle$ in the original (i.e. target) mixed state ρ.

IV. ENTANGLEMENT HAMILTONIAN IN STRONG INTER-CHAIN COUPLING LIMIT

We will derive the entanglement Hamiltonian H_E in the strong inter-chain coupling limit using perturbation theory. The starting point is the physical Hamiltonian:

$$\begin{aligned}
&\hat{H} = \hat{H}_A + \hat{H}_B + \hat{H}_{AB} \\
&\hat{H}_{\alpha=A(B)} = J_\parallel \sum_{\langle ij \rangle} [S^x_{i,\alpha} S^x_{j,\alpha} + S^y_{i,\alpha} S^y_{j,\alpha} + \Delta S^z_{i,\alpha} S^z_{j,\alpha}] \\
&\hat{H}_{AB} = J_\perp \sum_i [S^x_{i,A} S^x_{i,B} + S^y_{i,A} S^y_{i,B} + \Delta S^z_{i,A} S^z_{i,B}].
\end{aligned} \tag{42}$$

In the limit of $J_\perp \gg J_\parallel$, we treat $\hat{H}_{A(B)}$ as the perturbation to $\hat{H}_{AB}$. Thus the ground state of $\hat{H}_{AB}$ can be viewed as a product state of spin singlets:

$$|0\rangle = \prod_i |s_i\rangle, \tag{43}$$

where $|s_i\rangle$ is the spin singlet living on inter-chain bond:

$$|s_i\rangle = \frac{1}{\sqrt{2}}(|\uparrow_{i,A}\rangle|\downarrow_{i,B}\rangle - |\downarrow_{i,A}\rangle|\uparrow_{i,B}\rangle), \quad E_s = (-\frac{1}{2} - \frac{\Delta}{4})J_\perp \tag{44}$$

On each inter-chain bond, spin excitation state is described by spin triplet excitations:

$$\begin{aligned}
&|t^+_i\rangle = |\uparrow_{i,A}\rangle|\uparrow_{i,B}\rangle, \qquad E_{t^+} = \frac{\Delta}{4} J_\perp \\
&|t^0_i\rangle = \frac{1}{\sqrt{2}}(|\uparrow_{i,A}\rangle|\downarrow_{i,B}\rangle + |\downarrow_{i,A}\rangle|\uparrow_{i,B}\rangle), \quad E_{t^0} = (\frac{1}{2} - \frac{\Delta}{4})J_\perp \\
&|t^-_i\rangle = |\downarrow_{i,A}\rangle|\downarrow_{i,B}\rangle, \qquad E_{t^-} = \frac{\Delta}{4} J_\perp.
\end{aligned} \tag{45}$$

At first-order perturbation theory, the first-order correction is

$$\begin{aligned}
|1\rangle &= \sum_i |t^+_i t^-_{i+1}\rangle \frac{\langle t^+_i t^-_{i+1}|\hat{H}_A + \hat{H}_B|0\rangle}{E_+ + E_- - 2E_s} + |t^-_i t^+_{i+1}\rangle \frac{\langle t^-_i t^+_{i+1}|\hat{H}_A + \hat{H}_B|0\rangle}{E_- + E_+ - 2E_s} + |t^0_i t^0_{i+1}\rangle \frac{\langle t^0_i t^0_{i+1}|\hat{H}_A + \hat{H}_B|0\rangle}{2E_0 - 2E_s} \\
&= \frac{J_\parallel}{4J_\perp} \sum_i [\frac{2}{1+\Delta}|t^+_i t^-_{i+1}\rangle + \frac{2}{1+\Delta}|t^-_i t^+_{i+1}\rangle - \Delta|t^0_i t^0_{i+1}\rangle]
\end{aligned}$$

, where we use the notation:

$$\begin{aligned}
&|t^+_i t^-_{i+1}\rangle = |s_1\rangle \otimes ...|s_{i-1}\rangle|t^+_i\rangle|t^-_{i+1}\rangle \otimes |s_{i+2}\rangle ...|s_L\rangle \\
&|t^-_i t^+_{i+1}\rangle = |s_1\rangle \otimes ...|s_{i-1}\rangle|t^-_i\rangle|t^+_{i+1}\rangle \otimes |s_{i+2}\rangle ...|s_L\rangle \\
&|t^0_i t^0_{i+1}\rangle = |s_1\rangle \otimes ...|s_{i-1}\rangle|t^0_i\rangle|t^0_{i+1}\rangle \otimes |s_{i+2}\rangle ...|s_L\rangle
\end{aligned}$$

and Hamiltonian elements can be calculated by using:

$$\begin{aligned}
S^+_{i,A} S^-_{i+1,A}|s_i\rangle|s_{i+1}\rangle &= -\frac{1}{2}|t^+_i\rangle|t^-_{i+1}\rangle \\
S^-_{i,A} S^+_{i+1,A}|s_i\rangle|s_{i+1}\rangle &= -\frac{1}{2}|t^-_i\rangle|t^+_{i+1}\rangle \\
S^z_{i,A} S^z_{i+1,A}|s_i\rangle|s_{i+1}\rangle &= \frac{1}{4}|t^0_i\rangle|t^0_{i+1}\rangle
\end{aligned}$$

The reduced density matrix can be obtained by (within first-order perturbation approximation):

$$\rho_A = Tr_B[|\psi\rangle\langle\psi|] = Tr_B[(|0\rangle + |1\rangle)(\langle 0| + \langle 1|)] \tag{46}$$

First we get

$$
\begin{aligned}
Tr_B|0\rangle\langle 0| &= \prod_i Tr_B|s_i\rangle\langle s_i| \\
&= \prod_i [\langle\uparrow_i^B\ |s_i\rangle\langle s_i|\ \uparrow_i^B\rangle + \langle\downarrow_i^B\ |s_i\rangle\langle s_i|\ \downarrow_i^B\rangle] \\
&= \prod_i \frac{1}{2}[|\uparrow_i^A\rangle\langle\uparrow_i^A| + |\downarrow_i^A\rangle\langle\downarrow_i^A|] = \frac{1}{2^L}
\end{aligned}
$$

Second, we calculate

$$
\begin{aligned}
Tr_B[|1\rangle\langle 0| + |1\rangle\langle 0|] = \frac{J_\parallel}{4J_\perp}[&-\Delta Tr_B|t_i^0 t_{i+1}^0\rangle\langle 0| + \frac{2}{1+\Delta}Tr_B|t_i^+ t_{i+1}^-\rangle\langle 0| + \frac{2}{1+\Delta}Tr_B|t_i^- t_{i+1}^+\rangle\langle 0| + \\
&-\Delta Tr_B|0\rangle\langle t_i^0 t_{i+1}^0| + \frac{2}{1+\Delta}Tr_B|0\rangle\langle t_i^+ t_{i+1}^-| + \frac{2}{1+\Delta}Tr_B|0\rangle\langle t_i^- t_{i+1}^+|] \\
= -\frac{1}{2^L}\frac{J_\parallel}{4J_\perp}[&2\Delta 4S_i^z S_{i+1}^z + 4\frac{2}{1+\Delta}(S_i^+ S_{i+1}^- + h.c.)] \\
= -\frac{1}{2^L}\frac{4J_\parallel}{J_\perp(1+\Delta)}[&\frac{1}{2}\Delta(1+\Delta)S_i^z S_{i+1}^z + \frac{1}{2}(S_i^+ S_{i+1}^- + h.c.)]
\end{aligned}
$$

Here we use the following relations:

$$
\begin{aligned}
Tr_B|t_i^0 t_{i+1}^0\rangle\langle 0| = \frac{1}{2^{L-2}}[&\langle\uparrow_i^B\uparrow_{i+1}^B\ |t_i^0\rangle|t_{i+1}^0\rangle\langle s_i|\langle s_{i+1}|\ \uparrow_i^B\uparrow_{i+1}^B\rangle + \langle\downarrow_i^B\downarrow_{i+1}^B\ |t_i^0\rangle|t_{i+1}^0\rangle\langle s_i|\langle s_{i+1}|\ \downarrow_i^B\downarrow_{i+1}^B\rangle + \\
&\langle\uparrow_i^B\downarrow_{i+1}^B\ |t_i^0\rangle|t_{i+1}^0\rangle\langle s_i|\langle s_{i+1}|\ \uparrow_i^B\downarrow_{i+1}^B\rangle + \langle\downarrow_i^B\uparrow_{i+1}^B\ |t_i^0\rangle|t_{i+1}^0\rangle\langle s_i|\langle s_{i+1}|\ \downarrow_i^B\uparrow_{i+1}^B\rangle] \\
= \frac{1}{2^L}[&|\downarrow_i^A\downarrow_{i+1}^A\rangle\langle\downarrow_i^A\downarrow_{i+1}^A| + |\uparrow_i^A\uparrow_{i+1}^A\rangle\langle\uparrow_i^A\uparrow_{i+1}^A| - |\uparrow_i^A\downarrow_{i+1}^A\rangle\langle\uparrow_i^A\downarrow_{i+1}^A| - |\downarrow_i^A\uparrow_{i+1}^A\rangle\langle\downarrow_i^A\uparrow_{i+1}^A|] \\
= \frac{1}{2^L}&4S_i^z S_{i+1}^z
\end{aligned}
$$

and

$$
\begin{aligned}
Tr_B|t_i^+ t_{i+1}^-\rangle\langle 0| = \frac{1}{2^{L-2}}[&\langle\uparrow_i^B\uparrow_{i+1}^B\ |t_i^+\rangle|t_{i+1}^-\rangle\langle s_i|\langle s_{i+1}|\ \uparrow_i^B\uparrow_{i+1}^B\rangle + \langle\downarrow_i^B\downarrow_{i+1}^B\ |t_i^+\rangle|t_{i+1}^-\rangle\langle s_i|\langle s_{i+1}|\ \downarrow_i^B\downarrow_{i+1}^B\rangle + \\
&\langle\uparrow_i^B\downarrow_{i+1}^B\ |t_i^+\rangle|t_{i+1}^-\rangle\langle s_i|\langle s_{i+1}|\ \uparrow_i^B\downarrow_{i+1}^B\rangle + \langle\downarrow_i^B\uparrow_{i+1}^B\ |t_i^+\rangle|t_{i+1}^-\rangle\langle s_i|\langle s_{i+1}|\ \downarrow_i^B\uparrow_{i+1}^B\rangle] \\
= \frac{1}{2^L}[&-2|\uparrow_i^A\downarrow_{i+1}^A\rangle\langle\downarrow_i^A\uparrow_{i+1}^A|] \\
= \frac{1}{2^L}[&-2S_i^+ S_{i+1}^-]
\end{aligned}
$$

Third, we derive

$$
\begin{aligned}
Tr_B[|1\rangle\langle 1|] &= \sum_{i,j}\big(\frac{J_\parallel}{4J_\perp}\big)^2[\frac{2}{1+\Delta}|t_i^+t_{i+1}^-\rangle+\frac{2}{1+\Delta}|t_i^-t_{i+1}^+\rangle-\Delta|t_i^0t_{i+1}^0\rangle][\frac{2}{1+\Delta}\langle t_j^+t_{j+1}^-|+\frac{2}{1+\Delta}\langle t_j^-t_{j+1}^+|-\Delta\langle t_j^0t_{j+1}^0|] \\
&= \big(\frac{J_\parallel}{4J_\perp}\big)^2\sum_i[\frac{2^2}{(1+\Delta)^2}Tr_B|t_i^+t_{i+1}^-\rangle\langle t_{i+1}^+t_{i+2}^-|+\frac{2^2}{(1+\Delta)^2}Tr_B|t_i^+t_{i+1}^-\rangle\langle t_{i+1}^-t_{i+2}^+|-\frac{2\Delta}{1+\Delta}Tr_B|t_i^+t_{i+1}^-\rangle\langle t_{i+1}^0t_{i+2}^0| \\
&\quad \frac{2^2}{(1+\Delta)^2}Tr_B|t_i^-t_{i+1}^+\rangle\langle t_{i+1}^+t_{i+2}^-|+\frac{2^2}{(1+\Delta)^2}Tr_B|t_i^-t_{i+1}^+\rangle\langle t_{i+1}^-t_{i+2}^+|-\frac{2\Delta}{1+\Delta}Tr_B|t_i^-t_{i+1}^+\rangle\langle t_{i+1}^0t_{i+2}^0| \\
&\quad -\frac{2\Delta}{1+\Delta}Tr_B|t_i^0t_{i+1}^0\rangle\langle t_{i+1}^+t_{i+2}^-|-\frac{2\Delta}{1+\Delta}Tr_B|t_i^0t_{i+1}^0\rangle\langle t_{i+1}^-t_{i+2}^+|+\Delta^2Tr_B|t_i^0t_{i+1}^0\rangle\langle t_{i+1}^0t_{i+2}^0|] \\
&\quad +\big(\frac{J_\parallel}{4J_\perp}\big)^2[\frac{2^2}{(1+\Delta)^2}Tr_B|t_{i+1}^+t_{i+2}^-\rangle\langle t_i^+t_{i+1}^-|+\frac{2^2}{(1+\Delta)^2}Tr_B|t_{i+1}^+t_{i+2}^-\rangle\langle t_i^-t_{i+1}^+|-\frac{2\Delta}{1+\Delta}Tr_B|t_{i+1}^+t_{i+2}^-\rangle\langle t_i^0t_{i+1}^0| \\
&\quad \frac{2^2}{(1+\Delta)^2}Tr_B|t_{i+1}^-t_{i+2}^+\rangle\langle t_i^+t_{i+1}^-|+\frac{2^2}{(1+\Delta)^2}Tr_B|t_{i+1}^-t_{i+2}^+\rangle\langle t_i^-t_{i+1}^+|-\frac{2\Delta}{1+\Delta}Tr_B|t_{i+1}^-t_{i+2}^+\rangle\langle t_i^0t_{i+1}^0| \\
&\quad -\frac{2\Delta}{1+\Delta}Tr_B|t_{i+1}^0t_{i+2}^0\rangle\langle t_i^+t_{i+1}^-|-\frac{2\Delta}{1+\Delta}Tr_B|t_{i+1}^0t_{i+2}^0\rangle\langle t_i^-t_{i+1}^+|+\Delta^2Tr_B|t_{i+1}^0t_{i+2}^0\rangle\langle t_i^0t_{i+1}^0|] \\
&= \frac{1}{2^{L-3}}\big(\frac{J_\parallel}{4J_\perp}\big)^2[\frac{2^2}{(1+\Delta)^2}\frac{1}{2}(S_i^+S_{i+2}^-+h.c.)+\frac{\Delta^2}{8}42S_i^zS_{i+2}^z] \\
&= \frac{1}{2^L}\big(\frac{J_\parallel}{J_\perp}\big)^2\frac{1}{2}[\frac{2^2}{(1+\Delta)^2}\frac{1}{2}(S_i^+S_{i+2}^-+h.c.)+\Delta^2S_i^zS_{i+2}^z]
\end{aligned}
$$

And we need the relations:

$$Tr_B|t_i^0t_{i+1}^0\rangle\langle t_{i+1}^0t_{i+2}^0| = \frac{1}{8}4S_i^zS_{i+2}^z \tag{47}$$

$$Tr_B|t_i^+t_{i+1}^-\rangle\langle t_{i+1}^-t_{i+2}^+| = \frac{1}{2}|\uparrow_i^A\downarrow_{i+1}^A\downarrow_{i+2}^A\rangle\langle\downarrow_i^A\downarrow_{i+1}^A\uparrow_{i+2}^A| \tag{48}$$

$$Tr_B|t_i^-t_{i+1}^+\rangle\langle t_{i+1}^+t_{i+2}^-| = \frac{1}{2}|\downarrow_i^A\uparrow_{i+1}^A\uparrow_{i+2}^A\rangle\langle\uparrow_i^A\uparrow_{i+1}^A\downarrow_{i+2}^A| \tag{49}$$

$$Tr_B|t_{i+1}^+t_{i+2}^-\rangle\langle t_i^-t_{i+1}^+| = \frac{1}{2}|\uparrow_i^A\uparrow_{i+1}^A\downarrow_{i+2}^A\rangle\langle\downarrow_i^A\uparrow_{i+1}^A\uparrow_{i+2}^A| \tag{50}$$

$$Tr_B|t_{i+1}^-t_{i+2}^+\rangle\langle t_i^+t_{i+1}^-| = \frac{1}{2}|\downarrow_i^A\downarrow_{i+1}^A\uparrow_{i+2}^A\rangle\langle\uparrow_i^A\downarrow_{i+1}^A\downarrow_{i+2}^A| \tag{51}$$

$$\tag{52}$$

At last, we sum up all calculations together:

$$
\begin{aligned}
\rho_A &= Tr_B[(|0\rangle+|1\rangle)(\langle 0|+\langle 1|)] \\
&= \frac{1}{2^L}\big[1-\frac{4J_\parallel}{J_\perp(1+\Delta)}[\frac{1}{2}\Delta(1+\Delta)S_i^zS_{i+1}^z+\frac{1}{2}(S_i^+S_{i+1}^-+h.c.)]+\big(\frac{J_\parallel}{J_\perp}\big)^2\frac{1}{2}[\frac{2^2}{(1+\Delta)^2}\frac{1}{2}(S_i^+S_{i+2}^-+h.c.)+\Delta^2S_i^zS_{i+2}^z]\big] \\
&\approx \frac{1}{\mathcal{Z}}\exp(-\mathcal{H}_E^{per})
\end{aligned} \tag{53}
$$

, where

$$\mathcal{H}_E^{per} = \tilde{J}_1^{xy}\sum_{i,\alpha=x,y}S_i^\alpha S_{i+1}^\alpha+\tilde{J}_1^{zz}\sum_i S_i^zS_{i+1}^z-\tilde{J}_2^{xy}\sum_{i,\alpha=x,y}S_i^\alpha S_{i+2}^\alpha-\tilde{J}_2^{zz}\sum_i S_i^zS_{i+2}^z, \tag{54}$$

and $\tilde{J}_1^{xy}=\frac{4}{1+\Delta}\frac{J_\parallel}{J_\perp}$, $\tilde{J}_1^{zz}=2\Delta\frac{J_\parallel}{J_\perp}$, $\tilde{J}_2^{xy}=\frac{2}{(1+\Delta)^2}\big(\frac{J_\parallel}{J_\perp}\big)^2$ and $\tilde{J}_2^{zz}=\frac{\Delta^2}{2}\big(\frac{J_\parallel}{J_\perp}\big)^2$. Here we only keep the leading term in nearest neighbor and second nearest neighbor couplings. The form that we show in the main text is the case for isotropic case $\Delta=1$. The anisotropic form will be discussed in Sec. .

V. COMPARISON ENTANGLEMENT SPECTRA WITH EIGENVALUES SPECTRUM OF PARENT HAMILTONIAN

The equivalence between the entanglement Hamiltonian H_E and parent Hamiltonian H_P can be validated through the analysis of universal feature in the entanglement spectra (ES). Here we show the comparison of ES of entanglement Hamiltonian and

eigenvalue spectrum of parent Hamiltonian in spin ladder model (the results for 1D spin chain model has been shown in the main text). Fig. 5 shows typical ES (measured from the minimal value ξ_0) plotted as a function of momentum $K = \frac{2\pi k}{L}$ ($k = 0, 1, ..., L-1$), since the translational symmetry along the chain direction is preserved. For the isotropic case $\Delta = 1$ (Fig. 5(a)), the low-lying excitations of ES form an arch structure, which can be fitted by the des Cloiseaux-Pearson dispersion relations $\xi_i - \xi_0 = v|\sin K|$ (red dashed line). It strongly suggests the ES can resemble gapless quantum critical behavior which is intrinsic to the quantum spin$-1/2$ Heisenberg chain [17, 51]. Importantly, the eigenvalue spectra of obtained H_P shows the very similar features (Fig. 5(b)). As a direct comparison, we plot $\varepsilon_n - \varepsilon_0$ and $\xi_n - \xi_0$ ($\xi_n = -\log p_n$) in Fig. 5(c). It is found that eigenvalue ε_n has one-to-one correspondence with ξ_i, and a linear relationship $\varepsilon_n \propto \xi_n$ can be established (red dashed line). Here, the comparison between entanglement spectra and eigenvalue spectra of H_P clearly establishes the relationship between entanglement Hamiltonian and reduced density matrix: $H_E = f(H_P) \approx H_P$.

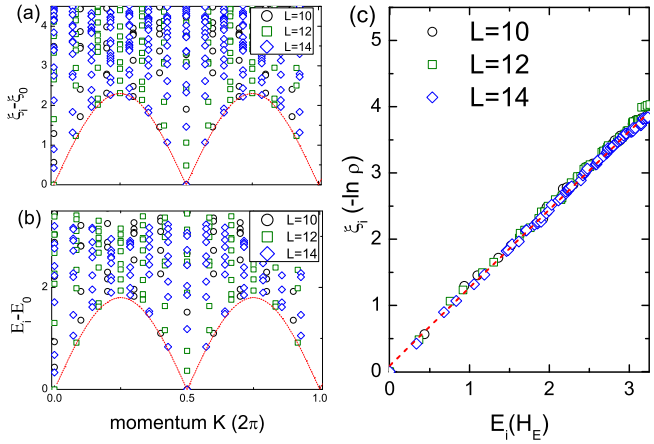

FIG. 5. (a) Entanglement spectra ($\xi_i - \xi_0$), obtained from reduced density matrix, are grouped by total momentum K along the chain direction. (b) Energy spectra ($E_i - E_0$) of reconstructed entanglement Hamiltonian H_E. In (a-b), the lowest spectra branch is fitted as $v|\sin K|$ by red dashed line. (c) Direct comparison of entanglement spectra ($\xi_i - \xi_0$) and energy spectra ($E_i - E_0$). All low-lying spectra are computed on $2 \times L$ ladders shown in black circles ($L = 10$), green squares ($L = 12$) and blue diamonds ($L = 14$). Here we set $\theta = \pi/3$ and $\Delta = 1.0$.

VI. ANISOTROPIC CASE

1. Spin ladder model

In the main text, we focus on the isotropic case in spin-ladder model. Here we briefly discuss the anisotropic case ($\Delta > 1$). In our extensive tests, our numerical scheme works well for both isotropic and anisotropic Heisenberg model. For the anisotropic case, we can also map out the entanglement Hamiltonian within the same scheme. Here we show spin ladder model (Fig. 1(b) of main text) and take $J_\perp/J_\parallel = 4$ and $\Delta = 2$ as an example:

$$\begin{aligned}
\hat{H} &= \hat{H}_A + \hat{H}_B + \hat{H}_{AB} \\
\hat{H}_{\alpha=A(B)} &= J_\parallel \sum_{\langle ij \rangle} [S^x_{i,\alpha} S^x_{j,\alpha} + S^y_{i,\alpha} S^y_{j,\alpha} + \Delta S^z_{i,\alpha} S^z_{j,\alpha}] \\
\hat{H}_{AB} &= J_\perp \sum_i [S^x_{i,A} S^x_{i,B} + S^y_{i,A} S^y_{i,B} + \Delta S^z_{i,A} S^z_{i,B}].
\end{aligned} \tag{55}$$

The targeting operator space is chosen to be:

$$\begin{aligned}
\mathcal{H}_E &= \sum_{n=1}^{N_r} J^{xy}_n \hat{h}^{xy}_n + J^{zz}_n \hat{h}^{zz}_n \\
\hat{h}^{xy}_n &= \sum_{i=1}^{L} (S^x_i S^x_{i+n} + S^y_i S^y_{i+n}), \;\; \hat{h}^{zz}_n = \sum_{i=1}^{L} S^z_i S^z_{i+n}.
\end{aligned} \tag{56}$$

Within the same scheme shown in the main text, the obtained parameters of entanglement Hamiltonian is shown in Tab. IV. As shown in Tab. IV, H_E breaks the spin rotation symmetry $J_n^{xy} \neq J_n^{zz}$. We also confirm that the parameters in H_E can be compared with perturbation theory as shown in the Sec. . These facts point to that H_E is effectively described by the XXZ spin chain with spin rotation symmetry breaking. This is not surprising since the parent Hamiltonian breaks spin rotation symmetry explicitly.

TABLE IV. Parameters of entanglement Hamiltonian H_E for anisotropic spin ladder model. Here we set $J_\perp/J_\parallel = 4$ and $\Delta = 2$.

L	g_0	J_1^{xy}	J_2^{xy}	J_1^{zz}	J_2^{zz}
10	1.34×10^{-8}	0.304	−0.039	0.952	−0.065
12	6.37×10^{-7}	0.299	−0.039	0.951	−0.061
14	8.89×10^{-7}	0.303	−0.038	0.950	−0.067

2. Spin chain model

For the spin chain model, we also study the entanglement Hamiltonian for anisotropic case $\Delta > 1$. The subsystem entanglement Hamiltonian is obtained in the same methodology as discussed in the main text. The coupling strength of entanglement Hamiltonian is shown in Fig. 6 for various Δ. Since the spin rotation system is breaking, we distinguish the longitudinal and transversal mode here. Generally, by increasing $\Delta > 1$, the longitudinal part dominates over the transversal mode. Another notable feature is the fluctuation around the entanglement boundary becomes apparent, which can be attributed to localized magnon quasiparticle around the open boundary. We also compare the results with the envelope function from the CFT (see main text) in Fig. 6. It is clear that, the entanglement Hamiltonian doesnot match the CFT prediction, especially for large Δ case. This can be understood that, in $\Delta > 1$ case, the low-energy effective theory is not CFT any more, thus the entanglement Hamiltonian does not satisfy the CFT form.

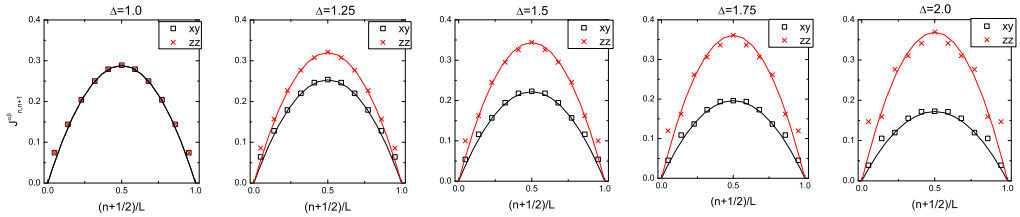

FIG. 6. Coupling strength of entanglement Hamiltonian of spin-1/2XXZ model: $\hat{H} = \sum_{n=1}^{2L} \hat{h}_{n,n+1} = \sum_{n=1}^{2L} S_n^x S_{n+1}^x + S_n^y S_{n+1}^y + \Delta S_n^z S_{n+1}^z$. Different panels show various $\Delta > 1$. The subsystem size is chosen to be $L_A = 12$. The squared dots and crossed dots respectively represent the longitudinal and transverse coupling strength $J_{n,n+1}^{zz}, J_{n,n+1}^{xy}$. The dashed lines show various envelope function for entanglement Hamiltonian $f_{CFT}(x) = B(L_A - x)x/L_A$ (B is a renormalized factor).